JCTC Journal of Chemical Theory and Computation

ARTICLE

pubs.acs.org/JCTC

Essential on the Photophysics and Photochemistry of the Indole Chromophore by Using a Totally Unconstrained Theoretical Approach

Angelo Giussani,*[,†] Manuela Merchán,[†] Daniel Roca-Sanjuán,*[,‡] and Roland Lindh[‡]

[†]Instituto de Ciencia Molecular, Universitat de València, Apartado 22085, ES-46071 Valencia, Spain

[‡]Department of Chemistry − Ångstrom, Theoretical Chemistry Program, Uppsala University Box 518, 75120 Uppsala, Sweden

Supporting Information

ABSTRACT: Indole is a chromophore present in many different molecules of biological interest, such as the essential amino acid tryptophan and the neurotransmitter serotonin. On the basis of CASPT2//CASSCF quantum chemical calculations, the photophysical properties of the system after UV irradiation have been studied through the exploration of the potential energy hypersurfaces of the singlet and triplet low-lying valence excited states. In contrast to previous studies, the present work has been carried out without imposing any restriction to the geometry of the molecule (C_1 symmetry) and by performing minimum energy path calculations, which is the only instrument able to provide the lowest-energy evolution of the system. Relevant findings to the photophysics of bare indole have been obtained, which compete with the currently accepted mechanism for the energy decay in the molecule. The results show the presence of a conical intersection (CI) between the initially populated $^1(L_a\ \pi\pi^*)$ and the $^1(L_b\ \pi\pi^*)$ state, easily accessible through a barrierless pathway from the Franck−Condon region. At this CI region, part of the population is switched from the bright $^1(L_a\ \pi\pi^*)$ state to the $^1(L_b\ \pi\pi^*)$ state, and the system evolves toward a minimum structure from which the expected fluorescence takes place. The reported low values of the fluorescence quantum yield are explained by means of a new nonradiative mechanism specific for the $^1(L_b\ \pi\pi^*)$ state, in which the presence of an ethene-like CI between the $(L_b\ \pi\pi^*)$ and ground states is the main feature.

INTRODUCTION

Due to their omnipresence in biological systems, the research on proteins has always been a field of enormous importance in almost every branch of bioscience. Regarding their photophysical properties, the main features of the near and far ultraviolet spectra of proteins have been reported in the regions between 220 and 190 nm (5.64−6.53 eV) and around 280 nm (4.43 eV).[1,2] This behavior is explained in terms of their constituents and in particular by the presence of aromatic amino acids [phenylalanine (Phe), tyrosine (Tyr), tryptophan (Trp), histidine (His)] whose photophysics determine the global response of proteins to UV radiation. Within the cited aromatic amino acids, the study of tryptophan has attracted special attention since it undoubtedly constitutes the most important emissive source in polypeptides, and its photophysical response is highly sensitive to the local microenvironment. The study of tryptophan is then relevant both to explain the global photophysics of many different proteins and to evaluate the potential of this amino acid as a useful probe of local environment and dynamics in proteins.[3] The chromophore group of tryptophan is indole (see Figure 1), which is also present in many different molecules of biological interest, like the neurotransmitter serotonin. A complete and correct description of the photophysical behavior of indole is consequently not only a matter of fundamental knowledge, but it constitutes the basis toward the understanding of the UV-induced processes taking place in more complicated related compounds.

Many experimental[4−20] and theoretical[21−27] studies have been performed on bare indole. The analysis of the gas-phase absorption spectrum of the molecule in the low-energy UV range has shown the contribution of two electronic transitions, one responsible for the sharp peak at 4.37 eV[4−8] and the other related to a broad continuum peaking around 4.77 eV.[7,9] These transitions have been assigned to two low-lying $\pi\pi^*$ valence singlet excited states which have been labeled, according to the Platt's nomenclature,[28] as $^1(L_b\ \pi\pi^*)$ and $^1(L_a\ \pi\pi^*)$. The $^1(L_a\ \pi\pi^*)$ state is characterized by a higher dipole moment, 5.4 D,[11] in comparison with the values for $^1(L_b\ \pi\pi^*)$ and the ground state, equal to 2.3[12] and 2.09 D,[13] respectively. Theoretical calculations were able to properly describe the absorption maxima measured in the experiments. Serrano-Andrés and Roos,[22] by using the complete active space self-consistent field/multiconfigurational second-order perturbation theory (CASSCF/CASPT2) methodology, reported the vertical excitation energies of the $^1(L_b\ \pi\pi^*)$ and $^1(L_a\ \pi\pi^*)$ states at 4.43 and 4.73 eV, respectively, in agreement with the experimental data. Regarding band origins, the value related to the $^1(L_b\ \pi\pi^*)$ state was identified by means of the analysis of the fluorescence excitation and emission spectra of the system and is considered to be coincident to the reported absorption maximum at 4.37 eV.[7] The $^1(L_a\ \pi\pi^*)$ band origin was more problematic, since its location was for a long time hampered by the vibronic structure of the $^1(L_b\ \pi\pi^*)$ state. Finally, the value was measured at 4.54 eV by means of site-selected fluorescence excitation in solid Ar matrices.[10] Such data have been also corroborated by the theoretical works of Serrano-Andrés, Roos, and Borin.[22,25]

Both theoretical and experimental studies on indole indicate that most of the molecules reach the $^1(L_a\ \pi\pi^*)$ state after UV

Received: September 15, 2011
Published: November 07, 2011

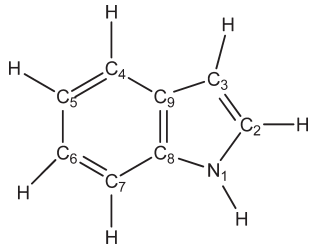

Figure 1. Indole structure and atom labeling.

irradiation. The oscillator strength (f) associated to the corresponding transition has been found to be larger than the value obtained for the $^1(L_b\ \pi\pi^*)$ state.[22,24] Subsequently, the population of the initially bright state is transferred to the $^1(L_b\ \pi\pi^*)$ state, as previously shown by Brand et al.,[20,21] which is expected to be the responsible for the fluorescence spectra of indole in the gas phase.[22] An interesting photophysical property of the system observed in the experiments is the dramatic decrease of the fluorescence quantum yield with the increase of the excitation energy.[14] This points out the presence of an efficient nonradiative decay path only accessible when the molecule is irradiated with an extra energy. In order to explain such behavior, Sobolewski, Domcke, and co-workers[23,26,27] proposed a nonradiative relaxation mechanism based on the topology of the potential energy hypersurfaces (PEHs) of a dark $\pi\sigma^*$ electronic state as a function of the proton-detachment coordinate of the NH group, which provides a plausible radiationless decay path whose importance has been also highlighted experimentally.[15,16]

Such global scenario of the radiative and nonradiative properties of indole has been accepted by many theoretical and experimental groups during the last decades, although a totally unconstrained theoretical research on the evolution of the initially populated $^1(L_a\ \pi\pi^*)$ state has not been carried out. Most of the cited works were in fact performed by constraining the molecule to planarity, i.e., imposing C_s symmetry, and no minimum energy paths (MEPs)[29,30] have been accounted for. In the studies carried out by Serrano-Andrés, Roos, and Borin,[22,24,25] the geometry for the emissive species was obtained by the standard optimization procedure, a strategy not able to show the presence or not any barrier between the Franck−Condon (FC) region and the excited-state minimum structures. On the other hand, Sobolewski, Domcke, and co-workers[23,26,27] explored the PEHs profile only along the proton-detachment coordinate of the NH group, through the optimization of different structures each with a fixed value of the NH bond distance.

In the present contribution, by using the current state-of-the-art computational strategies, we have obtained the unconstrained evolution of the system, allowing to relax all possible degrees of freedom of the molecule. The MEP technique with mass-weighted coordinates has been employed. This procedure is in fact the only computational tool able to describe the adiabatic evolution of a state, providing (if present) a steepest descendent path which consequently will constitute the most favorable decay experimented by the system. Our results clearly identify as primary process upon the population of the brightest excited state [the $^1(L_a\ \pi\pi^*)$ state] a switch to the lowest excited state $^1(L_b\ \pi\pi^*)$ driven by the presence of a conical intersection, reported recently by Brand et al.[20,21] In addition, the analysis performed without imposing any symmetry constraint to the system allows to find and characterize a nonradiative decay process particular to the $^1(L_b\ \pi\pi^*)$ state, which is mediated by an nonplanar ethene-like CI[31,32,39] between $^1(L_b\ \pi\pi^*)$ and the ground state. This radiationless decay path rationalizes the experimental observations, complementing the current established mechanism for energy-decay in the indole molecule, and contributes therefore to the elucidation of the global response of bare indole to UV radiation.

The results are presented in five sections. First, the low-lying singlet and triplet excited states involved in the photophysics of indole are analyzed. In the second section, evolution of the system after excitation to the brightest low-lying excited state without any excess energy is elucidated by the description of the so-called main decay path. Next, two additional decay paths are described. In section four, a new nonradiative decay mechanism specific for the $^1(L_b\ \pi\pi^*)$ state is considered in detail. Finally, the photophysics of the two low-lying triplet valence excited states is briefly discussed.

METHODOLOGY

The present study has been performed by using the well-tested CASPT2//CASSCF methodology[33−36] as implemented in the MOLCAS 7.4 software.[37] Optimized structures and minimum energy paths have been then calculated at the multiconfigurational CASSCF level, and at the geometries so obtained, the dynamic correlation effects have been taken into account in the energies by performing second-order multiconfigurational CASPT2 calculations. All computations have been performed by imposing no restrictions to the symmetry of the molecule (C_1 symmetry); out-of-plane geometry distortions were therefore allowed. Two basis sets of atomic natural orbital (ANO) of S- and L-type contracted to C,N [4s,3p,1d]/H[2s1p], have been employed resulting in similar conclusions. The results reported here correspond to the higher level of theory, that is, employing the latter basis set. The whole π system of the molecule has been considered in the active space. Thus, it comprises six π orbitals of the benzene ring plus two π orbitals of the pyrrole ring and the π orbital of the nitrogen atom, together with the corresponding 10 electrons [CASSCF(10,9)]. As the CASPT2//CASSCF methodology is strongly determined not only by the size of the active space but also by the shape of the orbitals employed, for the sake of clarity, a picture of the active orbitals is reported in Figure S1, Supporting Information. Within the CASPT2 calculations, an imaginary level-shift correction of 0.2 au has been used in order to avoid the presence of intruder states. The CASPT2 standard zeroth-order Hamiltonian has been used as originally implemented.[34] The core orbitals have been frozen in the CASPT2 calculations. Such CASPT2 approach has been validated during the last decades in many different studies on organic molecules providing a correct description and interpretation of the photophysical experimental data.[38,39] As highlighted above, research of the evolution of the valence excited states has been performed by means of MEP calculations.[29,30] Mass-weighted coordinates have been used. This technique provides (if present) a steepest descendent path, in which each step is built by the minimization of the energy on a hyperspherical cross section of the PEH centered on the initial geometry within a predefined radius. The importance and reliability of results obtained using such a computational tool have been proven in many different studies which confirm MEP calculations as a valuable procedure for the description of the photophysics and photochemistry of a molecule.[40,41] CIs not obtained along MEPs

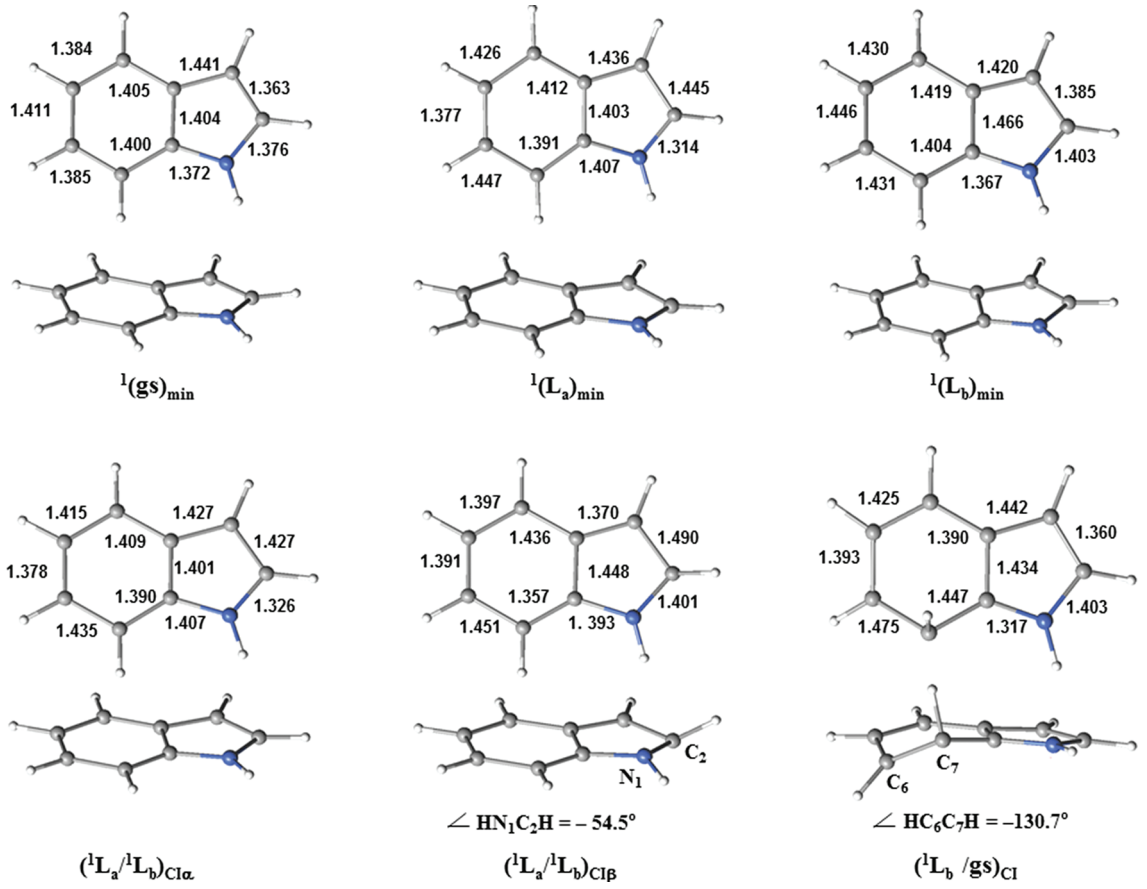

Figure 2. Frontal and side views of the CASSCF optimized structures of indole. CC and CN bond lengths (in Å) are also shown.

calculations have been computed by using the restricted Lagrange multipliers technique, as included in the MOLCAS 7.4 package in which the lowest-energy point is obtained under the restriction of degeneracy between the two considered states.[37]

RESULTS AND DISCUSSION

FC Geometry: Singlet and Triplet Valence Excited States. Optimization of the ground state of indole with a totally unconstrained approach leads to a planar geometry, labeled $^1(gs)_{min}$. The frontal and side views of this structure are depicted in Figure 2, and the most significant bond lengths and angles are compiled in Table 1. All these structural parameters are in agreement with previous results obtained by Serrano-Andrés and Roos.[22] At the geometry of this minimum, $^1(gs)_{min}$, a vertical CASPT2//CASSCF calculation of the low-lying six singlet excited states has been undertaken in order to study the absorption properties of the molecule in the FC region. For the sake of completeness, the lowest triplet excited states have been also computed. Only valence excited states have been considered since the present study is focused on the photophysics of indole, which is mainly determined by the valence electronic structure of the molecule. Analysis of nonpure valence excited states has been provided elsewhere.[22,23,26,27] For instance, Serrano-Andrés and Roos studied the nature of several low-lying excited states and the corresponding excitation energies by using extended basis sets, including Rydberg basis functions.[22] The two lowest excited states, which will be the ones studied in the present work, have been determined to be valence states. The analysis of the orbitals involved in the excitations related to these low-lying valence excited states has been carried out here to establish their nature. According to the Platt's nomenclature,[28] the valence states of interest can be described in terms of the natural orbitals (NOs) topologically equivalent to the highest occupied molecular orbital (HOMO) and lowest unoccupied molecular orbital (LUMO). Thus, the CASSCF wave function basically described by the minus linear combination of the HOMO (H) → LUMO (L) + 1 (25%) and H − 1 → L (47%) configurations is identified as the $^1(L_b\ \pi\pi^*)$ state, while the CASSCF wave function mainly composed by the H → L (56%) one-electron promotion is recognized as the $^1(L_a\ \pi\pi^*)$ state. The computed CASPT2 energies show that the $^1(L_b\ \pi\pi^*)$ and $^1(L_a\ \pi\pi^*)$ states are the lowest $\pi\pi^*$ valence singlet excited states, placed vertically (E_{VA}) at 4.36 and 4.79 eV, respectively (see Table 2). The results are in agreement with the available experimental data.[1,2,4,5,7,9] Table 3 compiles in addition the computed oscillator strengths (f) and dipole moments (μ) for the $^1(L_b\ \pi\pi^*)$ and $^1(L_a\ \pi\pi^*)$ states. According to the results, the latter is predicted to be the bright state upon UV irradiation. The calculated dipole moment, μ, at the FC region is also consistent with the experimental findings.[11−13] The $^1(L_b\ \pi\pi^*)$ state has a low μ (1.55 D), similar to the value obtained for the ground state (1.81 D), while $^1(L_a\ \pi\pi^*)$ is characterized by a high μ (6.07 D), which is more than three times larger with respect to the former.

Rydberg states are not described here, and for this reason, the basis set employed in our calculations does not include the

dx.doi.org/10.1021/ct200646r |J. Chem. Theory Comput. 2011, 7, 4088–4096

Table 1. Calculated and Experimental Bond Lengths and Angles for the Optimized Ground-State Geometry $^1(gs)_{min}$, the Conical Intersection $(^1L_a/^1L_b)_{CI\alpha}$, and the Equilibrium Geometry $^1(L_b)_{min}$ of the Indole Molecule

bonds[a]	$^1(gs)_{min}$[b]	$(^1L_a/^1L_b)_{CI\alpha}$	$^1(L_b)_{min}$[b]	exptl[c]	angles[a]	$^1(gs)_{min}$[b]	$(^1L_a/^1L_b)_{CI\alpha}$	$^1(L_b)_{min}$[b]	exptl[c]
N_1C_2	1.376	1.326	1.403	1.377	$N_1C_2C_3$	109.6	107.7	108.4	111.5
C_2C_3	1.363	1.427	1.385	1.344	$C_2C_3C_9$	106.7	106.8	107.8	105.5
C_3C_9	1.441	1.427	1.420	1.451	$C_3C_9C_4$	133.9	132.9	133.5	132.2
C_9C_4	1.405	1.409	1.419	1.412	$C_9C_4C_5$	118.9	116.9	118.0	114.6
C_4C_5	1.384	1.415	1.430	1.397	$C_4C_5C_6$	120.9	122.3	121.7	124.8
C_5C_6	1.411	1.378	1.446	1.386	$C_5C_6C_7$	121.2	121.5	120.8	119.7
C_6C_7	1.385	1.435	1.431	1.399	$C_6C_7C_8$	117.5	115.0	117.1	116.4
C_7C_8	1.400	1.390	1.404	1.400	C_8N_1H	125.7	124.1	125.0	
C_8N_1	1.372	1.407	1.367						
C_8C_9	1.404	1.401	1.466						
N_1H	0.990	0.997	0.989						

[a] Bonds are in Å and angles in degrees (°). [b] ANO-L type basis set C,N [4s,3p,1d]/H[2s1p], CASPT2//CASSCF(10,9) calculations. [c] Taken from the crystal X-ray structure for the ground state of tryptophan (ref 42).

Table 2. Calculated and Experimental Energy (in eV) for the Low-Lying Excited Valence States of the Isolated Indole Molecule

	theory			experiments[c]		
state	E_{VA}[a]	T_e[a]	E_{VE}[a]	A_{max}[b]	T_0[b]	R. emi[b]
$^1(L_b\ \pi\pi^*)$	4.36	4.11	4.01	4.37	4.37	4.12[e]/4.36
$^1(L_a\ \pi\pi^*)$	4.79	4.40	4.07	4.77	4.54	
$^3(L_a\ \pi\pi^*)$	3.42	3.01	2.68	3.3[d]	3.07[f]	2.87[f]
$^3(L_b\ \pi\pi^*)$	4.05	3.83	3.66			

[a] ANO-L type basis set C,N [4s,3p,1d]/H[2s1p], CASPT2//CASSCF-(10,9) vertical excitation energy (E_{VA}), electronic band origin (T_e), and vertical emission energy (E_{VE}). [b] Measured absorption band maximum (A_{max}), band origin (T_0), and relaxed emission from the excited-state relaxed geometry (R. emi). [c] Experiments from ref 1, 2, 4, 5, 7, and 9. [d] Estimated excitation energy from the ground state minimum (see ref 22). [e] Experiments from ref 17. [f] Experimental spectra from ref 18 and 19.

Table 3. Calculated Vertical Excitation Energies at the FC Geometry (E_{VA}, eV) for the Lowest Valence Singlet and Spin Forbidden Triplet Excited States[a]

root	state	E_{VA}	f	μ
S_0	gs			1.81
T_1	$^3(L_a\ \pi\pi^*)$	3.42		1.41
T_2	$^3(L_b\ \pi\pi^*)$	4.05		1.76
S_1	$^1(L_b\ \pi\pi^*)$	4.36	0.018	1.55
T_3	$^3(B_a\ \pi\pi^*)$	4.50		1.83
T_4	$^3(\pi\pi^*)$	4.74		1.46
T_5	$^3(B_b\ \pi\pi^*)$	4.76		5.08
S_2	$^1(L_a\ \pi\pi^*)$	4.79	0.078	6.07

[a] The computed dipole moments (μ, D) and the oscillator strengths (f) for the singlet−singlet transitions are also included.

required Rydberg-type functions to treat properly such states. Some calibration computations have been performed by locating at the center of mass Rydberg basis functions, which have been built specifically for the indole molecule (see Table S1, Supporting Information). The results obtained ensure an accurate description of the $^1(L_b\ \pi\pi^*)$ and $^1(L_a\ \pi\pi^*)$ states by means of the basis set without diffuse functions. In addition, the work carried out by Serrano-Andrés and Roos[22] on the theoretical study of the absorption spectrum of indole proved that the lowest Rydberg state appears vertically at 4.85 eV with respect to the ground-state energy, and our calculations show that only the $^1(L_b\ \pi\pi^*)$ and $^1(L_a\ \pi\pi^*)$ singlet excited states have a E_{VA} lower than 5.00 eV. Consequently, only the evolution of these two low-lying singlet valence excited states is analyzed in the next sections.

Regarding triplet excited states, the five low-lying computed roots present E_{VA} values lower than 5.00 eV, and therefore these states have been taken into account in the photochemical description of the system. As for the singlet excitations, the nature of the triplet states has been identified by inspection of the respective CASSCF wave functions, and each of them has been labeled by using Platt's nomenclature.[28] The overall results for the triplet states, together with those related to $^1(L_b\ \pi\pi^*)$ and $^1(L_a\ \pi\pi^*)$, are summarized in Table 3. In contrast to the singlet states, the $^3(L_a\ \pi\pi^*)$ has a lower E_{VA} than $^3(L_b\ \pi\pi^*)$, and both of them have dipole moments similar to that of the value obtained for the ground state.

Main Decay Path. From the analysis of the oscillator strength, it is possible to assert that most of the molecules reach the $^1(L_a\ \pi\pi^*)$ state after UV irradiation (the calculated f of the $^1(L_b\ \pi\pi^*)$ and $^1(L_a\ \pi\pi^*)$ states are 0.018 and 0.078, respectively). As stated above, from the FC geometry evolution of the initially populated $^1(L_a\ \pi\pi^*)$ state has been characterized by means of the MEP approach with no spatial symmetry constrains. The computational result is a barrierless path leading directly from the FC region to a CI involving the $^1(L_b\ \pi\pi^*)$ and $^1(L_a\ \pi\pi^*)$ states, placed at 4.42 eV with respect to the ground-state minimum, denoted hereafter as $(^1L_a/^1L_b)_{CI\alpha}$ (see Figure 3). Such degenerate region is a converged point on the obtained MEP, and it is not the lowest-energy point of the crossing seam but the first funnel that can be reached by the excited molecule, and consequently, the most photophysical relevant crossing point.[43] This CI has been characterized recently by Brand at al.[20,21] with an upper bound of around 4.6 eV at the DFT/MRCI level. An efficient internal conversion (IC) process mediated by this CI consequently causes the energy transfer from $^1(L_a\ \pi\pi^*)$ to $^1(L_b\ \pi\pi^*)$. Actually almost all the MEP points are characterized by a quite pronounced energy degeneracy between the $^1(L_b\ \pi\pi^*)$ and $^1(L_a\ \pi\pi^*)$ states, which suggests that along the decay pathway

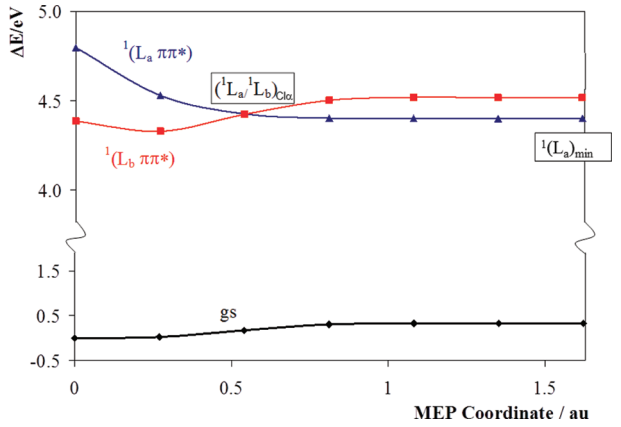

Figure 3. Evolution of the ground and two lowest singlet excited states for indole from the FC geometry along the $^1(L_a\ \pi\pi^*)$ MEP computed at the CASPT2//CASSCF(10,9)/ANO-L C,N [4s,3p,1d]/H[2s1p] level. The corresponding CASSCF MEP can be found in Figure S2, Supporting Information.

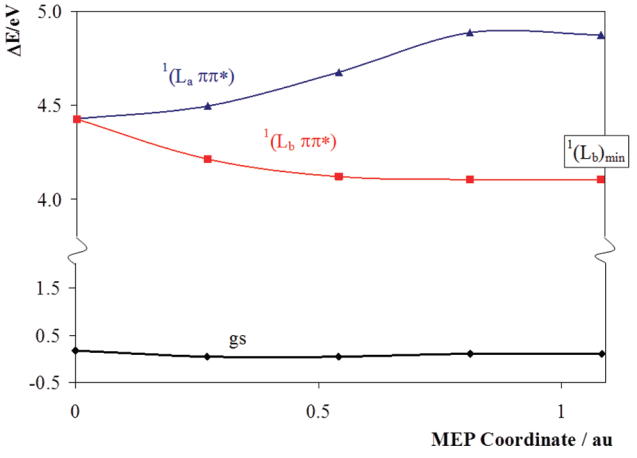

Figure 4. Evolution of the ground and two lowest singlet excited states for indole from the $(^1L_a/^1L_b)_{CI\alpha}$ conical intersection along the $^1(L_b\ \pi\pi^*)$ MEP computed at the CASPT2//CASSCF(10,9)/ANO-L C,N [4s,3p,1d]/H[2s1p] level. The corresponding CASSCF MEP can be found in Figure S3, Supporting Information.

from the FC region, the probability of populating the $^1(L_b\ \pi\pi^*)$ state is high. The equilibrium structure itself of the $^1(L_a\ \pi\pi^*)$ state, obtained as the last point of the MEP calculation, hereafter $^1(L_a)_{min}$, is placed at only 0.12 eV below $^1(L_b\ \pi\pi^*)$ state and is almost degenerated with the $(^1L_a/^1L_b)_{CI\alpha}$ point which mediates the ultrafast relaxation to the $^1(L_b\ \pi\pi^*)$ state. According to these findings, the $^1(L_a)_{min}$ structure, with a computed vertical emission (E_{VE}) of 4.07 eV (see Table 2), is not expected to contribute markedly to the fluorescence phenomenon in the indole molecule. This is in contrast with the initial evidence of dual fluorescence in both polar and nonpolar solvents, based on measurements of the polarization of the fluorescence bands,[44] and supports further experimental findings suggesting that, while two different states seem to contribute in the lowest-energy absorption band, only one of them is responsible for the emission.[2,45]

Figure 4 displays the results obtained for the MEP from $(^1L_a/^1L_b)_{CI\alpha}$. As can be seen in the picture, the $^1(L_b\ \pi\pi^*)$ state evolves through a steepest descendent path to the equilibrium geometry, $^1(L_b)_{min}$. Similar results are obtained by carrying out a MEP from the $^1(L_a)_{min}$ structure. At the $^1(L_b)_{min}$ geometry, the singlet excited state $^1(L_b\ \pi\pi^*)$ is the lowest on the S_1 hypersurface, and since the system cannot further evolve in a radiationless manner, we conclude that it is from this region that the emission takes place. For the S_1 state, the computed E_{VA}, the electronic band origin (T_e), and E_{VE} are 4.36, 4.11, and 4.01 eV, respectively (see Table 2). The present results agree within 0.26 eV with those obtained by Serrano-Andrés and Roos,[22] being particularly closer to the experimental data reported by Borisevich et al.[17] than to other initial observations.[7] In general all the theoretical and experimental studies result in lower E_{VA}, T_e, and E_{VE} values for $^1(L_b\ \pi\pi^*)$ with respect to the $^1(L_a\ \pi\pi^*)$ state.

The present optimized $^1(L_a)_{min}$, $(^1L_a/^1L_b)_{CI\alpha}$, and $^1(L_b)_{min}$ structures are almost planar (see Figure 2 and Table 1). In both $^1(L_a)_{min}$ and $(^1L_a/^1L_b)_{CI\alpha}$, the relative positions of the single and double bonds are interchanged with respect to $^1(gs)_{min}$. Meanwhile the $^1(L_b)_{min}$ geometry reflects electron delocalization taking place within the benzene ring.

Additional Decay Paths. In the previous section, the main decay path on the photophysics of indole has been characterized, i.e., the primary process that follows the population of the brightest excited state upon light irradiation. To improve the description, two other relevant deactivation paths have been studied and are next analyzed.

The first one is based on the fact that the $^1(L_b\ \pi\pi^*)$ singlet state can also be initially populated by UV absorption, since the computed f is not negligible. In order to study such possibility, a MEP on the $^1(L_b\ \pi\pi^*)$ singlet state has been computed starting from the FC structure (see Figures 5a). The final point of the MEP corresponds to the same region previously found along the main decay path: the $^1(L_b)_{min}$ structure. This new evidence confirms the relevant participation of the equilibrium structure of the $^1(L_b\ \pi\pi^*)$ state, $^1(L_b)_{min}$, in the fluorescence phenomenon of indole.

The second possible deactivation path studied involves an alternative CI between the $^1(L_a\ \pi\pi^*)$ and $^1(L_b\ \pi\pi^*)$ states, which will be denoted as $(^1L_a/^1L_b)_{CI\beta}$. This CI region might be important in the photophysics of indole since its energy with respect to the ground-state minimum is equal to 4.54 eV, which is only 0.12 eV above the former CI, $(^1L_a/^1L_b)_{CI\alpha}$. The new structure, $(^1L_a/^1L_b)_{CI\beta}$, is therefore placed in a region of the PEH energetically close to the main decay path that the system is expected to undertake upon absorption of UV light. As shown in Figure 2, $(^1L_a/^1L_b)_{CI\beta}$, in contrast to $(^1L_a/^1L_b)_{CI\alpha}$, is characterized by a pronounced out-of-plane distortion mainly localized on the HN_1 and C_2H groups of atoms; the dihedral angle related to these atoms is equal to −54.5°.

In order to establish the accessibility of this region, which would give us a hint on the relevance of the CI for the photophysics of the system, a linear interpolation of internal coordinates (LIIC) calculation has been performed on both the $^1(L_a\ \pi\pi^*)$ and the $^1(L_b\ \pi\pi^*)$ states between the FC and $(^1L_a/^1L_b)_{CI\beta}$ structures (see Figure 5b). Such a type of calculation is able to provide a connected path between two regions of the PEH, along with the corresponding (if present) barrier, which constitutes an upper bound to the energy required to reach the final geometry from the starting one. The so-computed energy barriers along the $^1(L_a\ \pi\pi^*)$ and $^1(L_b\ \pi\pi^*)$ manifolds from the FC region to the $(^1L_a/^1L_b)_{CI\beta}$ geometry are 0.43 and 0.26 eV, respectively. These values show that the $(^1L_a/^1L_b)_{CI\beta}$

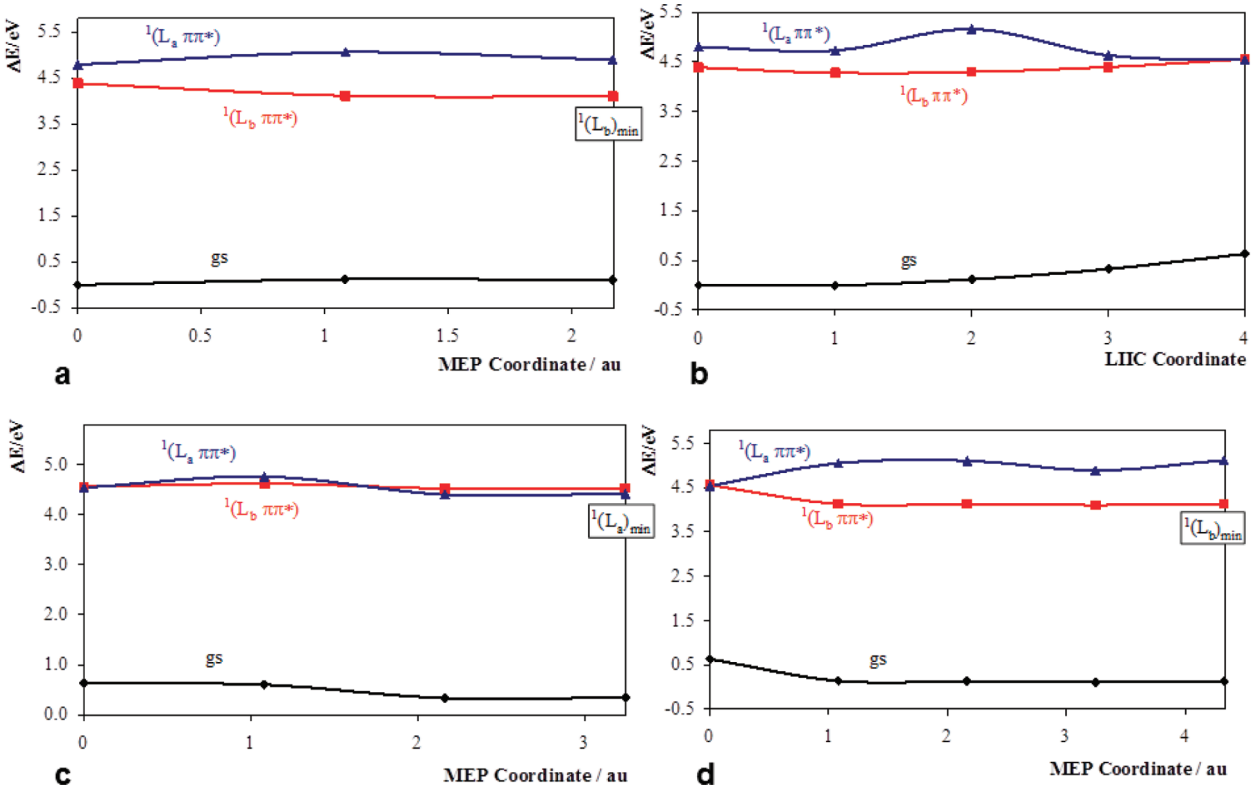

Figure 5. Energy profiles of the ground and two lowest singlet excited states for indole along the additional decay paths computed at the CASPT2//CASSCF(10,9)/ANO-L C,N [4s,3p,1d]/H[2s1p] level: (a) $^1(L_b\ \pi\pi^*)$ MEP from the FC geometry, $^1(gs)_{min}$; (b) LIIC between $^1(gs)_{min}$ and $(^1L_a/^1L_b)_{CI\beta}$; (c) $^1(L_a\ \pi\pi^*)$ MEP from $(^1L_a/^1L_b)_{CI\beta}$; and (d) $^1(L_b\ \pi\pi^*)$ MEP from $(^1L_a/^1L_b)_{CI\beta}$. The corresponding CASSCF MEPs can be found in Figures S4−S6, Supporting Information, respectively.

region might be accessible after UV-irradiation at least from the $^1(L_b\ \pi\pi^*)$ state. An energy barrier of 0.1−0.2 eV is in fact normally considered a small barrier, although only dynamics studies of the system can actually provide such conclusion.

According to the suggested plausible accessibility of the $(^1L_a/^1L_b)_{CI\beta}$ region upon UV irradiation, the evolution of the system from this CI has been also studied to give a complete description of the photophysics of bare indole. A MEP calculation shows that the $^1(L_a\ \pi\pi^*)$ state will evolve from the $(^1L_a/^1L_b)_{CI\beta}$ region to the previously characterized $^1(L_a)_{min}$ structure (see Figure 5c). Although the path on the $^1(L_a\ \pi\pi^*)$ PEH connecting the structures has been obtained through the use of the MEP technique, the correction introduced in energies by means of the CASPT2 computations results in a small barrier of 0.22 eV. This result further points out the importance of taking into account the correlation effects associated with the instantaneous short-range electron−electron interaction in order to give a correct description of excited-state PEHs. Due to the low value of the barrier obtained at the CASPT2 level, we conclude that the $^1(L_a\ \pi\pi^*)$ state will decay to the $^1(L_a)_{min}$ structure, from which, as previously stated, the system might evolve to the $^1(L_b)_{min}$ equilibrium geometry. For the sake of completeness, from the $(^1L_a/^1L_b)_{CI\beta}$ point the behavior of the $^1(L_b\ \pi\pi^*)$ state has also been studied by means of computing the corresponding MEP (Figure 5d). The evolution of the $^1(L_b\ \pi\pi^*)$ state from the $(^1L_a/^1L_b)_{CI\beta}$ region leads to an equilibrium geometry which belongs again to the region on the PEH of S_1 previously identified as responsible for the fluorescence produced by the system: the $^1(L_b)_{min}$ emissive structure.

In summary, all the secondary photophysical events analyzed, derived from the population of the $^1(L_b)$ state at the FC region or from the access of the $(^1L_a/^1L_b)_{CI\beta}$ structure after light absorption, drive the system toward the equilibrium region on the S_1 PEH, $^1(L_b)_{min}$, which is assigned the fluorescence feature of bare indole.

Nonradiative Decay Process toward the Ground State. We have shown that the photophysics of indole is characterized by different decay paths leading to the $^1(L_b)_{min}$ equilibrium structure, from which the molecule is predicted to emit light. Nevertheless, the intensity of the fluorescence band has been observed in several experiments to be sensitive to the excitation energy and the experimental conditions. In particular, the fluorescence quantum yield of bare indole drastically decreases as the excitation energy provided to the system increases.[14] The loss of fluorescence emission in bare indole was previously explained by Sobolewski, Domcke, and co-workers[23,26,27] who have shown that the presence of a dark $\pi\sigma^*$ state could be the responsibility of a nonradiative decay mechanism. According to their results, in order to activate such a radiationless process, the initially populated $^1(L_a\ \pi\pi^*)$ state has to reach a CI with the $\pi\sigma^*$ state which is placed above 5.00 eV with respect to the ground-state minimum. The authors then concluded that such barrier could explain the decrease of the fluorescence quantum yield of the system as the excitation energy is increased and predicted a threshold for this photophysical process to be located at about 5 eV for excitation from the minimum of the ground state. This mechanism is consistent with the increase of the nonradiative decay rate measured for indole with respect to

dx.doi.org/10.1021/ct200646r |J. Chem. Theory Comput. 2011, 7, 4088–4096

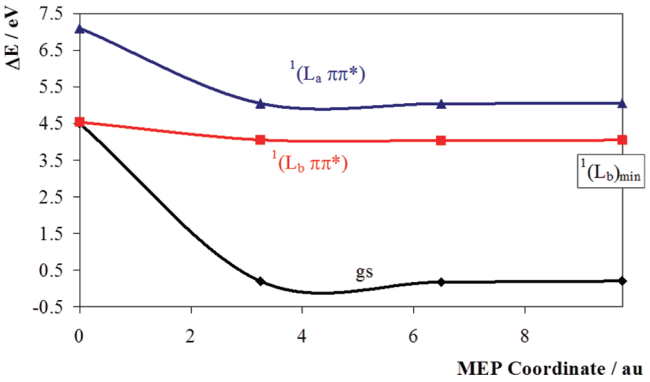

Figure 6. Evolution of the ground and two lowest singlet excited states for indole from the $(^1L_b/gs)_{CI}$ conical intersection along the $^1(L_b\ \pi\pi^*)$ MEP computed at the CASPT2//CASSCF(10,9)/ANO-L C,N [4s,3p,1d]/H[2s1p] level. The corresponding CASSCF MEP can be found in Figure S7, Supporting Information.

N-methylindole.[14] However, it does not account for other experimental observations. The emission quantum yield of indole after excitation to the $^1(L_a\ \pi\pi^*)$ state at 257.2 nm (4.81 eV) is equal to 0.103,[14] which is too low in comparison to the band intensity observed when excitation energies corresponding to the $^1(L_b\ \pi\pi^*)$ band origin are employed or to the present computational results.[7] In fact, Ilich concluded in the experimental work on the low-lying singlet states of indole that the system has remarkable emission features only for energies around the $^1(L_b\ \pi\pi^*)$ band origin (measured at 4.37 eV), whereas a 22-fold decrease is observed when the molecule is provided with an extra energy of 4200 cm^{-1} (0.52 eV).[7] Such experimental observations seem to point out the presence of a nonradiative decay path accessible for excitation energies lower that 5.00 eV and related to the $^1(L_b\ \pi\pi^*)$ state, apart from the radiationless route characterized by Sobolewski, Domcke, and co-workers.[23,26,27]

Consistent with these experimental findings, we have found a CI between $^1(L_b\ \pi\pi^*)$ and the ground state, denoted hereafter as $(^1L_b/gs)_{CI}$. This degenerate region is placed at 4.50 eV with respect to $^1(gs)_{min}$ and is characterized by a strong out-of-plane distortion, mainly localized on the C_6H and C_7H group of atoms (see Figure 2). Such a crossing point has some geometrical similarities with the so-called triangular/kink S_1/S_0 CI reported for polyenes and aromatic systems,[46,47] but it does not have the same electronics characteristics (three weakly coupled π-electrons on the out-of-plane distortion and a fourth electron localized along the remaining part of the benzene ring). It can be in fact better classified as a typical ethene-like CI,[31,32,39] in which a twist of the double bond between the C_6 and C_7 atoms leads to an out-of-plane deformation with a HC_6C_7H dihedral angle of $-127.1°$ and a pyramidalization of the C_7 atom. In order to determine the relevance of this CI on the photophysics of indole, a MEP on the S_1 state has been computed from the $(^1L_b/gs)_{CI}$ region (see Figure 6). This calculation shows the presence of a barrierless path leading to the $^1(L_b)_{min}$ region, which proves that $(^1L_b/gs)_{CI}$ can be reached from the equilibrium geometry of the $^1(L_b\ \pi\pi^*)$ state by overcoming a barrier of 0.39 eV. Such processes consequently constitute a nonradiative decay path specific for the $^1(L_b\ \pi\pi^*)$ state, whose accessibility depends on the energy provided to the system and can be activated at excitation energies lower than 5.00 eV.

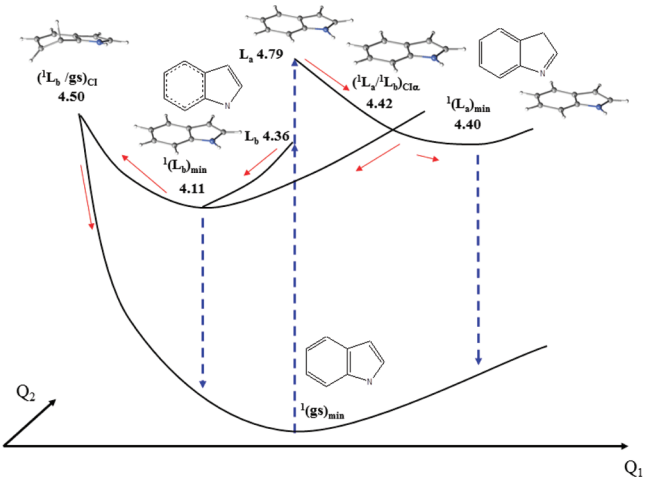

Figure 7. Scheme of the photophysics of indole along the singlet manifold. Energies (in eV) relative to the ground-state minimum structure, $^1(gs)_{min}$, are given. The Q_1 reaction coordinate is mainly related to the simple/double-bond rearrangements keeping the planarity of the molecule, meanwhile Q_2 is associated to out-of-plane distortions.

Figure 7 displays a scheme of the main decay paths after population of the $^1(L_a\ \pi\pi^*)$ and $^1(L_b\ \pi\pi^*)$ states at the FC region, together with the radiationless path mediated by $(^1L_b/gs)_{CI}$. The relative position of the latter CI with respect to the other singular points depicted in the figure supports the decrease of the measured fluorescence quantum yield with the increase of the excitation energy. After population of the bright $^1(L_a\ \pi\pi^*)$ state at the FC structure, the system has enough energy (~0.3 eV) to activate the nonradiative process via $(^1L_b/gs)_{CI}$, which is in agreement with relatively low fluorescence quantum yield observed by Glasser and Lami.[14] If the indole molecule is irradiated with a light energy similar to the $^1(L_b\ \pi\pi^*)$ band origin, the $^1(L_b)_{min}$ region may be directly populated and the system will need an extra energy of 0.40 eV to access the $(^1L_b/gs)_{CI}$ funnel to the ground state. Therefore, the fluorescence from the $^1(L_b)_{min}$ will be the predominant process taking place. The nonradiative energy decay to the ground state will begin to compete with the emission of light as the irradiation energy approaches the $^1(L_a\ \pi\pi^*)$ vertical excitation energy, which is located 0.29 eV above the $(^1L_b/gs)_{CI}$ structure.

On the basis of our results, we associate therefore the nonradiative process observed at energies below 5.00 eV to be determined mainly by the above-described path from the $^1(L_b)_{min}$ minimum structure to the ground state via the $(^1L_b/gs)_{CI}$, which implies a threshold for the photophysical process around 0.5 eV lower with respect to the mechanism proposed by Sobolewski, Domcke, and co-workers[23,26,27] and does not involve a dissociative $\pi\sigma^*$ state. It is worth mentioning however that the last energy decay route is still present to some extent, as it has been shown in some experiments in which the NH bond dissociation is observed,[15,16] and it might also contribute at excitation energies lower that 5.00 eV via tunneling effects. In order to determine the percentage in which this dissociative deactivation path competes with the new mechanism obtained, and in particular, to ultimately understand the respective contribution of both energy decay paths to the photophysics of the system depending on the excited state populated and on the exceeding energy provided, a quantum dynamics study on bare indole would be necessary. Up to now only on-the-fly molecular

mechanic simulation based on time-dependent density functional theory (TDDFT) calculations starting on the S_2 state have been performed.[48] In such work, some trajectories computed using the PBE functional actually decay through the $\pi\sigma^*$ state, giving a low quantum yield for the dissociation along the NH coordinate. Nevertheless, according to the authors results and comments, the PBE functional is not able to provide the correct ordering of the $^1(L_a\ \pi\pi^*)$ and $^1(L_b\ \pi\pi^*)$ states and the use of the CAM-B3LYP functional, which on the contrary gives the correct ordering of the low-lying excited states, and provides a larger energy gap between the $\pi\pi^*$ and $\pi\sigma^*$ states, decreasing the probability of energy decay via the mechanism involving the NH bond stretch.

Triplet States. Along the evolution of the initially populated $^1(L_a\ \pi\pi^*)$ singlet state, and through the subsequent $^1(L_b\ \pi\pi^*)$ steepest descendent path leading to the $^1(L_b)_{min}$ structure, no strongly efficient intersystem crossing regions have been identified. The same result has been obtained from the inspection of the two characterized secondary decay paths. In order to search for the phosphorescence structures related to the low-lying triplet excited states, $^3(L_a\ \pi\pi^*)$ and $^3(L_b\ \pi\pi^*)$, geometry optimizations of these states have been then carried out starting from the FC region. The minima obtained, namely $^3(L_a)_{min}$ and $^3(L_b)_{min}$, respectively, have an almost planar geometry (the corresponding structures can be found in Table S2, Supporting Information). The computed results, vertical excitation energies, band origins, and vertical emission energies are compiled in Table 2, together with the relevant experimental data. The $^3(L_a\ \pi\pi^*)$ state corresponds to the lowest triplet excited state at both the optimized $^3(L_a)_{min}$ and $^3(L_b)_{min}$ structures, and consequently the phosphorescence of the system is expected to take place from the $^3(L_a\ \pi\pi^*)$ state. In fact, a single phosphorescence band has been reported starting at 3.07 eV with a maximum at 2.87 eV,[18,19] which is in agreement with previous[22] and present theoretical findings for the $^3(L_a\ \pi\pi^*)$ state (see Table 2).

CONCLUSIONS

On the basis of the exploration of the PEH on the low-lying singlet and triplet excited states by means of accurate state-of-the-art computational strategies, a global and comprehensive description of the photophysics of bare indole under UV irradiation is provided. Two types of processes have been identified and characterized in the molecule after excitation to the low-lying singlet valence excited states $^1(L_a\ \pi\pi^*)$ and $^1(L_b\ \pi\pi^*)$: radiative and nonradiative energy decays. After UV absorption most of the molecules reach the bright $^1(L_a\ \pi\pi^*)$ excited state, which would evolve through a steepest descendent path toward a CI implying the $^1(L_b\ \pi\pi^*)$ state, mediating in this manner the energy transfer to the latter state. The relaxed structure $^1(L_b)_{min}$ on the S_1 hypersurface might be accessed subsequently and from this region the fluorescence emission takes place. All the secondary energy decay paths studied also lead to the emissive state, $^1(L_b)_{min}$. A radiationless decay specific to the $^1(L_b\ \pi\pi^*)$ state has been predicted involving a nonplanar ethene-like CI between $^1(L_b\ \pi\pi^*)$ and the ground state. According to the obtained pathways profiles, the process is inhibited at the energy around the $^1(L_b\ \pi\pi^*)$ band origin and becomes competitive with the fluorescence emission at excitation energies close the $^1(L_a\ \pi\pi^*)$ band maximum. The current findings explain for the first time the low fluorescence quantum yield measured experimentally after excitation to energy lower that 5.00 eV because of the presence of a not previously reported nonradiative decay mechanism specific for the $^1(L_b\ \pi\pi^*)$ state. No efficient intersystem crossings have been found along the decay paths analyzed, while the phosphorescence properties are in agreement with previous theoretical and experimental studies.

Two additional comments are appropriate at this final stage. First, as many other organic molecules, the nonradiative decay to the ground state of excited indole is mediated by the presence of an ethene-like CI. For instance, the photostability of the natural purines and pyrimidines nucleobases has been proven to be determined by the presence of easily accessible ethene-like CI, which provides the molecules with nonradiative paths to release the absorbed energy in an ultrafast manner.[31,32,49−54] The present study on the photophysics of bare indole further highlights the importance of such type of degenerate regions, which can be considered nowadays as a well-established concept in the field of efficient nonradiative decay funnels of organic systems. Second, since the topology of indole and the canonical nucleobase 9H-adenine are similar, that is, they are both built as six- and five-fused rings and the molecules have the same energetic ordering of the lowest $^1(L_b\ \pi\pi^*)$ and $^1(L_a\ \pi\pi^*)$ states at the FC region, the photophysics of 9H-adenine[49−53] might be compared with the results obtained here. The presence of a main nonradiative decay path toward the ground state, after excitation to the bright state, associated with an ethene-like CI appears as a common feature between the two systems, although involving the $^1(L_b\ \pi\pi^*)$ and $^1(L_a\ \pi\pi^*)$ states in indole and 9H-adenine, respectively. This can be ascribed to the different nature of the double bond implied in the CI of indole and 9H-adenine ($C_6{=}C_7$ versus $C_2{=}N_3$) and can consequently be related to the intrinsic nature of the two molecules.

ASSOCIATED CONTENT

Supporting Information. The natural orbitals of the active space employed in the CASSCF/CASPT2 calculations are depicted in Figure S1. Table S1 compiles the CASPT2 E_{VA} of indole at the FC geometry computed with two different basis sets including or not Rydberg functions. The CASSCF MEPs related to Figures 3−6, and corresponding to the $^1(L_a\ \pi\pi^*)$ MEP from the FC structure, $^1(L_b\ \pi\pi^*)$ MEPs from $(^1L_a/^1L_b)_{CI\alpha}$ and the FC geometry, $^1(L_a\ \pi\pi^*)$ MEP from $(^1L_a/^1L_b)_{CI\beta}$, and $^1(L_b\ \pi\pi^*)$ MEPs from $(^1L_a/^1L_b)_{CI\beta}$ and $(^1L_b/gs)_{CI}$ are displayed in Figures S2−7, respectively. The *x*, *y*, *z* coordinates for the structures of the present study can be found in Table S2. This material is available free of charge via the Internet at http://pubs.acs.org.

AUTHOR INFORMATION

Corresponding Author

*E-mail: Angelo.Giussani@uv.es; Daniel.Roca@kvac.uu.se.

ACKNOWLEDGMENT

Research supported by the project CTQ2010-14892 of the Spanish MEC/FEDER and the Swedish Research Council. A.G. gratefully acknowledges Ph.D. fellowship "V segles" from the Universitat de València. A.G. also thanks Prof. N. Ferré for useful discussion. D.R.-S. thanks European Research Council under the European Community's Seventh Framework Programme (FP7/2007-2013)/ERC grant agreement 255363.

REFERENCES

(1) Wetlaufer, D. B. Ultraviolet spectra of proteins and amino acids. In *Advances in Protein Chemistry*; Anfinsen, C. B., Anson, M. L., Bailey, K., Edsall, J. T., Eds.; Academic Press: New York, 1962; Vol. 17.

(2) Demchenko, A. P. *Ultraviolet Spectroscopy of Proteins*; Springer-Verlag: Berlin, 1986.

(3) Creed, D. *Photochem. Photobiol.* **1984**, *39*, 537.

(4) Hollas, J. M. *Spectrochim. Acta* **1963**, *19*, 753.

(5) Lami, H. *J. Chem. Phys.* **1977**, *67*, 3274.

(6) Lami, H. *Chem. Phys. Lett.* **1977**, *48*, 447.

(7) Ilich, P. *Can. J. Spectrosc.* **1987**, *67*, 3274.

(8) Bartis, T. L. O.; Grace, L. I.; Dunn, T. M.; Lubman, D. M. *J. Phys. Chem.* **1993**, *97*, 5820.

(9) Strickland, E. H.; Horwitz, J.; Billups, C. *Biochemistry* **1970**, *25*, 4914.

(10) Fender, B. J.; Sammeth, D. M.; Callis, P. R. *Chem. Phys. Lett.* **1995**, *239*, 31.

(11) Lami, H.; Glasser, N. *J. Chem. Phys.* **1986**, *84*, 597.

(12) Chang, C. T.; Wu, C. Y.; Muirhead, A .R.; Lombardi, J. R. *Photochem. Photobiol.* **1974**, *19*, 347.

(13) Caminati, W.; Di Bernardo, S. *J. Mol. Struct.* **1990**, *240*, 253.

(14) Glasser, N.; Lami, H. *J. Chem. Phys.* **1981**, *74*, 6526.

(15) Lin, M. F.; Tseng, C. M.; Lee, Y. T.; Ni, C. K. *J. Chem. Phys.* **2005**, *123*, 124303.

(16) Nix, M. G. D.; Devine, A. L.; Cronin, B.; Ashfold, M. N. R. *Phys. Chem. Chem. Phys.* **2006**, *8*, 2610.

(17) Borisevich, N. A.; Sukhodola, A. A.; Tolstorozhev, G. B. *Chem. Phys.* **2008**, *354*, 44.

(18) Zuckich, J.; von Schütz, J. U.; Maki, A. M. *J. Am. Chem. Soc.* **1974**, *96*, 710.

(19) Wilkinson, F.; Garmer, A. *J. Chem. Soc., Faraday Trans. 2* **1977**, *73*, 222.

(20) Brand, C.; Küpper, J; Pratt, D. W.; Meerts, W. L.; Krügler, D.; Tatchen, J.; Schmitt, M. *Phys. Chem. Chem. Phys.* **2010**, *12*, 4968.

(21) Küpper, J; Pratt, D. W.; Meerts, W. L.; Brand, C.; Tatchen, J.; Schmitt, M. *Phys. Chem. Chem. Phys.* **2010**, *12*, 4980.

(22) Serrano-Andrés, L.; Roos, B. O. *J. Am. Chem. Soc.* **1996**, *118*, 185.

(23) Sobolewski, A. L.; Domcke, W. *Chem. Phys. Lett.* **1999**, *315*, 293.

(24) Borin, A. C.; Serrano-Andrés, L. *Chem. Phys.* **2000**, *262*, 253.

(25) Serrano-Andrés, L.; Borin, A. C. *Chem. Phys.* **2000**, *262*, 267.

(26) Sobolewski, A. L.; Domcke, W.; Dedonder-Lardeux, C.; Jouvet, C. *Phys. Chem. Chem. Phys.* **2002**, *4*, 1093.

(27) Sobolewski, A. L.; Domcke, W. *J. Phys. Chem. A* **2007**, *111*, 11725.

(28) Platt, J. R. *J. Chem. Phys.* **1949**, *17*, 489.

(29) De Vico, L.; Olivucci, M.; Lindh, R. *J. Chem. Theory Comput.* **2005**, *1*, 1029.

(30) Anglada, J. M.; Bofill, J. M. *J. Comput. Chem.* **1997**, *18*, 992.

(31) Merchán, M.; González-Luque, R.; Climent, T.; Serrano-Andrés, L.; Rodríguez, E.; Reguero, M.; Peláez, D. *J. Phys. Chem. B* **2006**, *110*, 26471.

(32) Serrano-Andrés, L.; Merchán, M.; Borin, A. C. *J. Am. Chem. Soc.* **2008**, *130*, 2473.

(33) Andersson, K.; Malmqvist, P.-Å.; Roos, B. O. *J. Chem. Phys.* **1992**, *96*, 1218.

(34) Roos, B. O.; Andersson, K.; Fülscher, M. P.; Malmqvist, P.-Å.; Serrano-Andrés, L.; Pierloot, K.; Merchán, M. *Adv. Chem. Phys.* **1996**, *93*, 219.

(35) Serrano-Andrés, L.; Merchán, M. Spectroscopy: Applications. In *Encyclopedia of Computational Chemistry*; Schleyer, P. v. R., Schreiner, P. R., Schaefer, H. F., III, Jorgensen, W. L., Thiel, W., Glen, R. C., Eds., Wiley, Chichester, 2004, pp 1−51.

(36) Roca-Sanjuán, D.; Aquilante, F.; Lindh, R. *Wiley Interdiscip. Rev.: Comput. Mol. Sci.* **2011**; DOI: 10.1002/wcms.97.

(37) Aquilante, F.; De Vico, L.; Ferré, N.; Ghigo, G.; Malmqvist, P.−Å.; Pedersen, T.; Pitonak, M.; Reiher, M.; Roos, B. O.; Serrano-Andrés, L.; Urban, M.; Veryazov, V.; Lindh, R. *J. Comput. Chem.* **2010**, *31*, 224.

(38) Merchán, M.; Serrano-Andrés, L. Ab Initio Method for Excited States. In *Computational Photochemistry*, 1st ed.; Olivucci, M., Ed.; Elsevier: Amsterdam, The Netherlands, 2005; Vol. 16, pp 35−91.

(39) Serrano-Andrés, L.; Merchán, M. Photostability and Photoreactivity in Biomolecules: Quantum Chemistry of Nucleic Acid Base Monomers and Dimers. In *Radiation Induced Molecular Phenomena in Nucleic Acids*; Leszczynski, J., Shukla, M., Eds.; Springer: Heidelberg, The Netherlands, 2008; pp 435−472.

(40) Garavelli, M. *Theor. Chem. Acc.* **2006**, *116*, 87.

(41) Garavelli, M.; Bernardi, F.; Cembran, A. Ab Initio Method for Excited States. In *Computational Photochemistry*, 1rd ed.; Olivucci, M., Ed.; Elsevier: Amsterdam, The Netherlands, 2005; Vol. 16, pp 191−223.

(42) Takigawa, T.; Ashida, T.; Sasado, Y.; Kakuda, M. *Bull. Chem. Soc. Jpn.* **1966**, *39*, 2369.

(43) Michl, J. In *Computational Photochemistry*, 1rd ed.; Olivucci, M., Ed.; Elsevier: Amsterdam, The Netherlands, 2005; Vol. 16, pp ix−xi.

(44) Song, P. S.; Kurtin, W. E. *J. Am. Chem. Soc.* **1969**, *91*, 4892.

(45) Eftink, M. R. Fluorescence techniques for studying protein structure. In *Methods of Biochemical Analysis*; Suelter, C. H., Ed.; John Wiley & Sons: New York, 1991; Vol. 35.

(46) Garavelli, M.; Celani, P.; Yamamoto, N.; Bernardi, F.; Robb, M. A.; Olivucci, M. *J. Am. Chem. Soc.* **1996**, *118*, 11656.

(47) Garavelli, M.; Bernardi, F.; Cembran, A.; Castaño, O.; Frutos, L. M.; Merchán, M.; Olivucci, M. *J. Am. Chem. Soc.* **2002**, *124*, 13770.

(48) Wohlgemuth, M.; Bona i-Koutecký, V.; Mitrić, R. *J. Chem. Phys.* **2011**, *135*, 054105.

(49) Perun, S.; Sobolewski, A. L.; Domcke, W. *J. Am. Chem. Soc.* **2004**, *127*, 6257.

(50) Blancafort, L. *J. Am. Chem. Soc.* **2006**, *128*, 210.

(51) Serrano-Andrés, L.; Merchán, M.; Borin, A. C. *Chem.—Eur. J.* **2006**, *12*, 6559.

(52) Serrano-Andrés, L.; Merchán, M.; Borin, A. C. *Proc. Natl. Acad. Sci. U.S.A.* **2006**, *103*, 8691.

(53) Conti, I.; Garavelli, M.; Orlandi, G. *J. Am. Chem. Soc.* **2009**, *131*, 16108.

(54) Gobbo, J. P.; Borin, A. C.; Serrano-Andrés, L. *J. Phys. Chem. B* **2011**, *115*, 6243.